Applications of Surface Science 3 (1979) 13–37

THE APPLICATION OF HIGH-FIELD SURFACE ANALYTICAL TECHNIQUES TO THE STUDY OF PLASMA–WALL INTERACTIONS IN PLT *

G.L. KELLOGG and J.A. PANITZ
Sandia Laboratories **, *Albuquerque, New Mexico 87185, USA*

Received 17 May 1978
Revised manuscript received 31 August 1978

The techniques of imaging atom-probe mass spectroscopy, field-ion microscopy, and transmission electron microscopy have been used to analyze the surface and near-surface regions of field-emitter samples exposed to the plasma of the Princeton Large Torus (PLT) tokamak. The experiments were carried out to determine the extent of damage to the emitter surfaces resulting from plasma exposure, the composition and thickness of films deposited on the sample surfaces during irradiation, and the depth distribution of implanted plasma and impurity species in the near-surface region of the specimens. The analyses indicate that very little structural damage occurs to the wall of PLT as a result of impinging particles traveling in a direction perpendicular to the toroidal magnetic field lines within the tokamak, but that a considerable amount of limiter material is deposited on the wall surface during operation. The deposited layer was found only when the sample was directly exposed to the plasma; control specimens which were in the reactor at the same time but shielded from direct plasma exposure remained free of deposits.

1. Introduction

One of the limiting factors in achieving the plasma temperatures required for an "ignition" in present-day and near-future tokamaks is the problem of impurity contamination of the plasma [1]. It has been generally accepted that the source of these impurities is the tokamak first wall and/or limiters, but little is known about the specific mechanisms responsible for removing material from the wall or limiter surface and causing it to enter the plasma. Several possible mechanisms which could cause an impurity influx into the plasma of an operating tokamak include: (1) physical or chemical sputtering of wall material or adsorbed species on the wall surface, (2) photo-desorption of adsorbed atoms, (3) blistering of wall material, and (4) evaporation or fragmentation of the limiter. Other mechanisms are also possible [2].

---

* This work was supported by the U.S. Department of Energy (DOE), Office of Energy Technology Magnetic, under Contract AT(29-1)789 and carried out in cooperation with S.A. Cohen and H.F. Dylla at the Plasma Physics Laboratory in Princeton.

** A U.S. Department of Energy Facility.

In order to determine which mechanisms are important with respect to the plasma impurity situation (and ultimately to eliminate the problem by an appropriate choice of wall/limiter material and/or coating), a fairly substantial effort has been undertaken to try to characterize the plasma–first wall interaction in operating tokamaks.

A major contribution to this overall investigation has been made by the analysis of samples placed at the first wall of the various tokamaks during operation using a number of surface and near-surface sensitive techniques. Information relating to both structural and compositional changes at the first-wall surface can be obtained by using the different microscopic and spectroscopic techniques currently available, including transmission electron microscpy (TEM), scanning electron microscopy (SEM), scanning Auger microscopy (SAM), Auger electron spectroscopy (AES), secondary ion mass spectroscopy (SIMS), soft X-ray appearance potential spectroscopy (SXAPS), Rutherford ion backscattering (RIBS), electron stimulated desorption (ESD), and thermal desorption mass spectroscopy (TDMS) [3]. The information from these studies has been used to determine both how the plasma affects the first wall and how the first wall affects the plasma, thereby helping to elucidate the mechanisms which contribute to the plasma contamination problem in operating reactors.

We wish to report here on a recent investigation of plasma–wall interactions in which we have used the imaging atom-probe mass spectrometer (IAP) [4], the field-ion microscope (FIM) [5], and the scanning-transmission electron microscope (STEM) [6] to analyze the surface and near-surface region of field-emitter specimens which were placed at the position of the wall in the Princeton Large Torus (PLT) tokamak. There are several advantages in using high-field techniques rather than the more conventional techniques listed in the preceding paragraph. First, and of primary importance, is their sensitivity to both structural and compositional changes occurring at the sample surface. It has been estimated that the energy of escaping plasma species and impurities in present-day tokamaks is of the order of 100 eV [7]. Clearly, the implantation depth of these species into the first wall will be very limited, probably on the order of tens of ångströms for amorphous materials and extending to possibly several hundred ångströms for clean, crystalline materials where channeling is possible [8]. The ability of the FIM and IAP to detect structural and compositional features on essentially an atomic scale makes these instruments ideally suited to this type of investigation. Panitz [9] has demonstrated in an earlier experiment with an 80 eV deuterium ion source that it is possible to obtain very accurate depth distributions of low energy implanted species using the imaging atom-probe. For example, the depth distribution of deuterium implanted into single crystal (110) tungsten was observed to be highly structured when measured with a depth resolution of 2 Å. Currently, such depth resolution is not available with any other "surface sensitive" technique. These laboratory measurements also raised the interesting possibility of determining the energy distribution of escaping plasma species by comparing their depth distribution (obtained following irradiation in an operating tokamak) with a sequence of depth distributions measured in the laboratory for identical species, at various implantation energies [9].

An additional advantage offered by the imaging atom-probe technique is its ability to unambiguously detect hydrogen and its isotopes (deuterium and tritium), which are of primary interest in fusion reactor investigations. Other techniques which can detect these species (SIMS, RIBS) usually suffer from a lack of depth resolution (≈100 Å). A final advantage, which will become evident later, results from a combination of IAP and STEM analysis. Changes in the morphology of sample surfaces resulting from plasma exposure can be directly determined from TEM images of field emitters taken before and after irradiation in a tokamak. If a contaminant layer is deposited on a sample during plasma exposure, the thickness of the layer can be precisely determined to within the resolution capability of the STEM. This procedure eliminates the ambiguity inherent in other techniques which rely on sputter-removal of deposited layers to determine layer thicknesses.

2. Experimental techniques

The primary surface analytical techniques used in this study were imaging atom-probe mass spectroscopy, field-ion microscopy, and scanning-transmission electron microscopy. Both the field-ion microscope and the electron microscope are well-established instruments [5,6] and therefore will not be reviewed in this paper. The imaging atom-probe mass spectrometer, on the other hand, is a relatively new instrument, and the presentation of the data in the following sections will be facilitated by a brief description of the technique as it relates to the present investigation. More detailed reviews are available in the literature [4,10].

Fig. 1 shows, schematically, the main components of an IAP spectrometer. The specimen is a sharply-pointed field-emitter "tip" whose apex radius is, typically, of the order of several hundred ångströms. A mass spectrum of species residing on the specimen surface is obtained in the following manner. A field desorption [*] event is initiated by the application of a high voltage pulse, V_p, to the emitter. In order for the resulting electric field at the emitter surface to be large enough to initiate field-desorption, an additional dc bias voltage, V_{dc}, may be required. The total emitter potential ($V_{dc} + V_p$) produces an electric-field at the surface of the tip apex which removes species as positive ions. The ions are accelerated into a field-free region of length L, where they drift with energy $ne(V_{dc} + V_p)$. Here, n is the charge state of the desorbed ions. After a time t, the ions intercept a suitable imaging detector [4] allowing their total flight time to be recorded. The mass-to-charge ratio of the ions is then given by [4]

$$m/n = (2e/L^2)(V_{dc} + V_p)t^2 . \tag{1}$$

---

[*] Field-desorption is the physical process in which species are removed as positive ions from the surface of a metallic solid in a high electric field. Field evaporation is a term applied specifically to field-desorption of the lattice atoms of the solid.

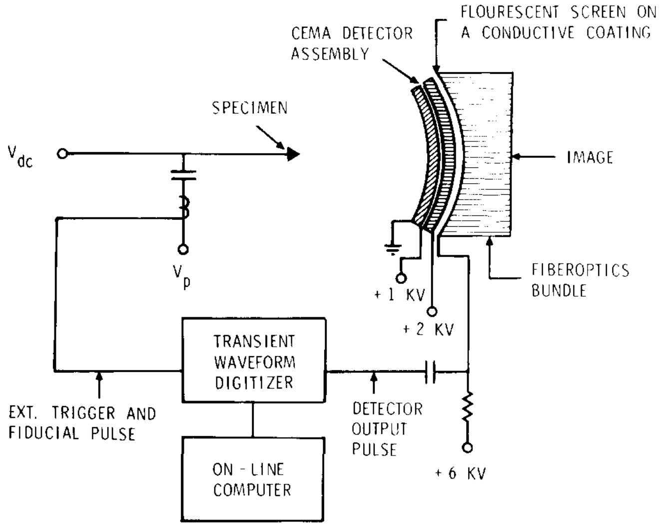

Fig. 1. Schematic drawing showing the essential components of an imaging atom-probe mass spectrometer.

The ion travel time is measured from the sweep of a Tektronix R7912 transient waveform digitizer which records a fiducial pulse corresponding in time to the application of the desorption pulse and the output signal of the detector, which corresponds to the arrival time of the species (see fig. 1). The difference in time between the two pulses is the travel time of the ion, if the small acceleration time between the tip and the drift region is neglected. When several different species on the emitter surface are desorbed simultaneously, they will arrive at the detector consecutively in time according to their mass-to-charge ratios. The amplitude of each resulting mass "peak" corresponds to the abundance of that particular species on the emitter surface. Since absolute abundances will depend upon many factors (including detection sensitivity and the extent to which all surface species are removed as positive ions), only relative abundances can be determined with accuracy.

The detector assembly also allows one to view the image of the desorbed ions as they intercept the channel plates. Thus, the spatial distribution of the desorbed species can also be determined. By observing the successive collapse of low index net planes (e.g. the (110) plane of tungsten) while field evaporating the lattice, the depth from the surface corresponding to each desorption event can be accurately measured in terms of the known interplanar lattice spacing. As mentioned earlier, depth distributions of implanted species with essentially ångström resolution can be obtained by using this "built-in" depth scale.

Species residing on the surface of a field emitter are usually found to field-desorb well below the evaporation field of the lattice. This allows one to determine the identity of species which have been deposited on the emitter surface by pulse-desorption at low fields. Problems can arise, however, when thick layers are deposited on the emitter surface, a situation which will be discussed later in this paper.

3. Experimental procedures and results

Two sets of eight field emitter samples were exposed in PLT at different times and were subsequently analyzed for structural and compositional changes at the surface. Since the exposure conditions and method of analysis were different for each sample set, the two experiments will be discussed separately in the following sections.

3.1. Sample set #1

The experiment involving the first set of samples was performed primarily as an attempt to establish the feasibility of using high-field techniques to study in situ irradiated samples in tokamaks, as previously proposed [11]. The principal objectives were: (1) to determine whether or not the delicate field emitter tips could survive exposure to an operating tokamak environment, (2) to determine if structural or compositional changes could be detected at the surface or in the near-surface region of the samples, and (3) to obtain depth distributions of implanted plasma species in the near surface region of the irradiated samples. Eight tungsten specimens were employed for this study. The reasons for choosing tungsten rather than an actual candidate wall material (e.g. stainless steel) were threefold. First, the sample preparation procedure, the field-ion imaging conditions, and the field-desorption techniques have all been well-established for tungsten. Second, many present-day tokamaks employ tungsten as a limiter which is directly exposed to the plasma during operation. And, finally, it has been found experimentally that tungsten does not form hydrides or deuterides in the high-field conditions present during field-desorption mass analysis [12]. This last consideration is extremely important with respect to acquiring accurate depth distributions of implanted plasma species, because any hydrogen or deuterium present has hydrides or deuterides within the sample would not be resolvable from their parent species in the imaging atom-probe.

Of the eight field emitters in the first set, only four had direct line-of-sight exposure to the PLT plasma. Fig. 2 shows a schematic drawing of the holder used for both transporting the samples to PLT and securing them during in situ exposure. The electrolytically-etched wire specimens were spot-welded to short (8.0 mm long, 1.5 mm dia.) stainless steel rods and secured in holes forming a circular pattern about the axis of a cylindrically shaped stainless steel block. A stainless steel cap was placed over the samples for protection against accidental damage in handling. To allow exposure to the plasma, four 1.5 mm holes were located in the cap directly above four of the specimens. The other four samples were shielded from direct plas-

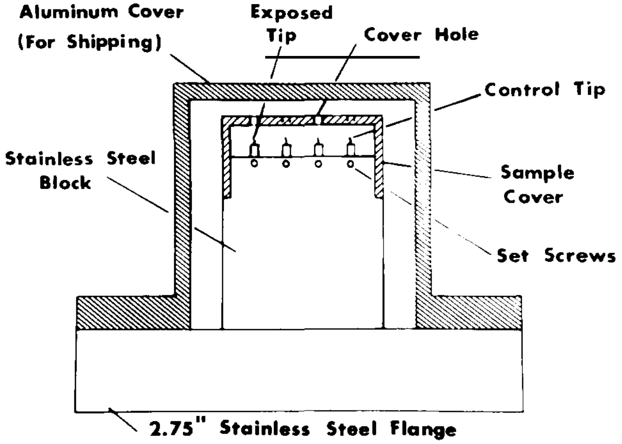

Fig. 2. Schematic drawing of the sample holder used for transporting the specimens to and from PLT and for securing the specimens during plasma exposure.

ma exposure and served as experimental controls, allowing the effects of exposure to the plasma and exposure to laboratory and/or PLT ambient to be distinguished.

After characterizing their surfaces by field-ion microscopy, the eight tungsten emitters were sent to Princeton where they were placed in PLT at the first-wall position for the two month period between April and May of 1977. The samples were positioned at the midplane of the torus, slightly recessed into the first wall, with the axis of the wire specimens approximately parallel to the major axis of the torus. A tungsten limiter was located approximately 160° around the torus from the tips. The samples were exposed to $\approx 10^4$ low power hydrogen discharge cleaning pulses and $\approx 3 \times 10^3$ high power deuterium and hydrogen discharge operation pulses during this two month period. Following the exposure, the samples were returned and analyzed by field-ion microscopy and imaging atom-probe mass spectroscopy.

Field-ion images of the shielded (control) tips (labeled 1, 3, 5, and 7) taken both before and after plasma exposure are shown in fig. 3a. The difference in resolution between the "before" and "after" micrographs in the figure is due to different field-ion imaging temperatures*. It is evident from the micrographs that no major structural changes occurred at the surfaces of any of the samples shielded from direct plasma exposure**.

---

* The "before" images were obtained with a FIM using a standard liquid nitrogen "cold finger" which did not allow specimen temperatures below 80 K. The "after" micrographs were taken on a different system which employed a closed-cycle liquid helium refrigerator with a maximum specimen temperature of 26 K defined by the low-power heater being used at the time of analysis.

** The field-ion image of tip #3 taken after PLT exposure also showed no evidence of damage, however, the tip "jumped" before a photograph could be taken. (Field stresses sometimes cause the tip to be destroyed during imaging, a process known as "tip jumping".)

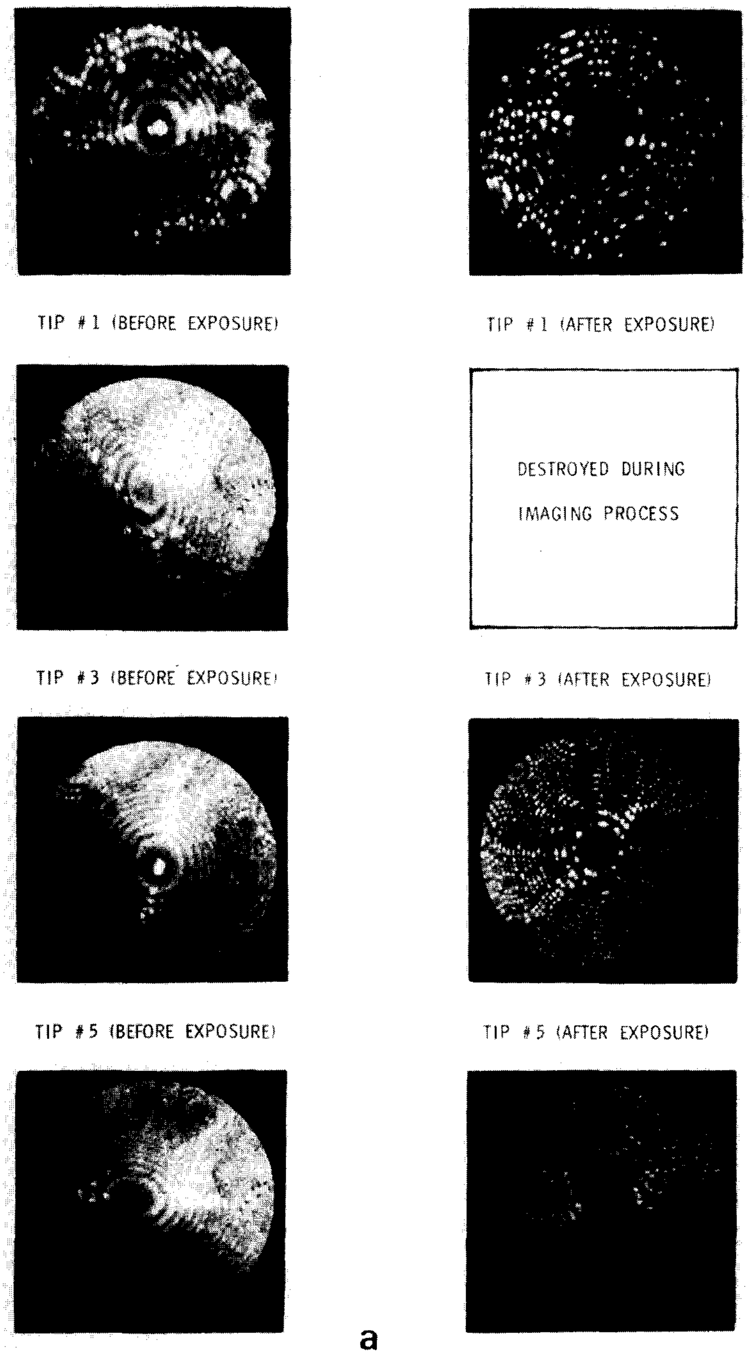

TIP #1 (BEFORE EXPOSURE)

TIP #1 (AFTER EXPOSURE)

TIP #3 (BEFORE EXPOSURE)

DESTROYED DURING IMAGING PROCESS

TIP #3 (AFTER EXPOSURE)

TIP #5 (BEFORE EXPOSURE)

TIP #5 (AFTER EXPOSURE)

TIP #7 (BEFORE EXPOSURE)

a

TIP #7 (AFTER EXPOSURE)

Fig. 3.(a) Field-ion micrographs of the shielded (control) tips of set #1 taken before and after exposure in PLT. The emitters were imaged in He at 80 K (before) and 26 K (after). No evidence for any structural damage is seen.

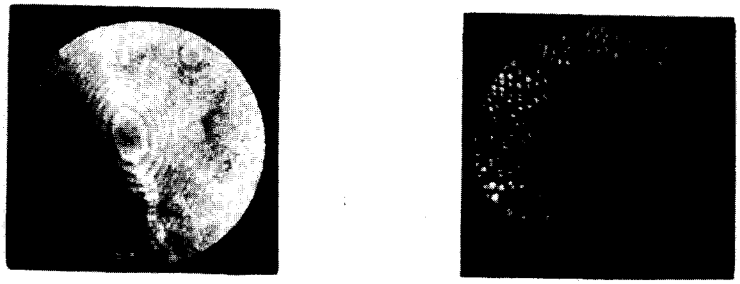

TIP #2 (BEFORE EXPOSURE)

TIP #2 (AFTER EXPOSURE)

TIP #4 (BEFORE EXPOSURE)

TIP #4 (AFTER EXPOSURE)

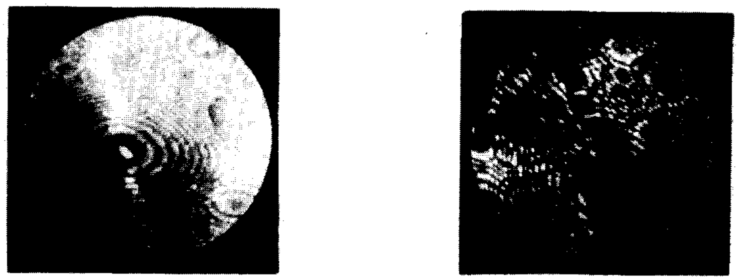

TIP #6 (BEFORE EXPOSURE)

TIP #6 (AFTER EXPOSURE)

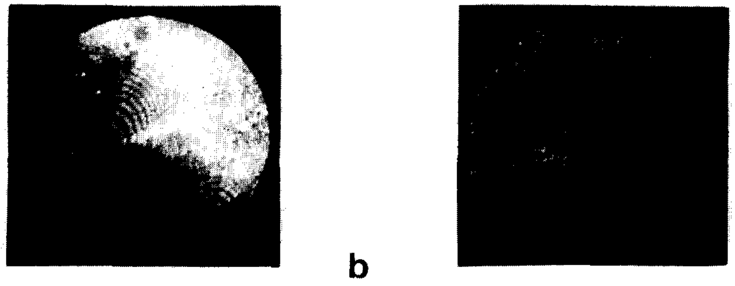

TIP #8 (BEFORE EXPOSURE)

TIP #8 (AFTER EXPOSURE)

Fig. 3.(b) Field-ion micrographs of the exposed tips of set #1 taken before and after exposure in PLT. The imaging conditions were the same as in fig. 3a. In this case, all four specimens are seen to have undergone some degree of damage from exposure to the plasma.

Fig. 3b shows the "before" and "after" field-ion images of the exposed tips. Here, all four of the samples have undergo some surface damage due to exposure in PLT. The dark region in the center of the image of tip #2 suggests that a portion of the end of the emitter has been removed. Although seen less extensively in tips #4 and #8, some atomic rearrangement at the surface has also occurred, and tip #6 is seen to have developed a grain boundary at the surface which was not present in the ion image before irradiation. The fact that all of the exposed and none of the shielded samples suffered some degree of lattice damage demonstrated that structural rearrangement on an atomic scale had occurred as a result of exposure to the PLT operation and/or cleaning cycles.

The ability to field-ion image the exposed sample surfaces (fig. 3b) in itself indicated that the extent of the damage caused by exposure in PLT was not excessive. One can further estimate the depth of structural rearrangement in the specimens by analyzing the field-ion images. An upper estimate for the damage depth into tip #8 can be obtained very easily because the damaged region is well-defined within a complete field-ion image. Each successive "ring" beginning at the central dark (110) plane in the field-ion image represents a plane of atoms which is one (110) layer deeper into the lattice. By counting the number of rings from the central (110) plane to a point beyond the region of damage ($\approx$18 in tip #8) and multiplying this number by the (110) interplanar spacing of 2.2 Å, one can determine the maximum damage depth ($\approx$40 Å for tip #8). Estimating the extent of damage for the other exposed samples is not quite as easy because the damage makes it impossible to count the number of rings in the central portion of the image. However, by measuring the difference in the radius of the tip (using the standard field-ion ring counting method [5]) both before exposure and after having field evaporated through the damaged region, it is possible to determine an upper value for the damage depth. For tip #2 (the most severely damaged) the radius difference is found to be $\approx$150 Å. Unfortunately, this method relies strongly on the shape (apex cone angle) of the emitter, which was not known in this initial experiment. As a result, the measurement is probably uncertain to ±100 Å. The minor damage found to take place in tip #8, however, suggests that the depth of the damaged region probably lies towards the lower end of the range (i.e. $\approx$50 Å).

Field-desorption mass spectra were obtained and used to determine the identity of species on the surface, within the damaged region, and into the near-surface region of the samples. The measurements revealed the presence of hydrogen, deuterium, carbon, oxygen, tungsten, and oxides of tungsten both on the surface and within the damaged region of the exposed tips. However, no evidence of implanted plasma species was found in the lattice eventually exposed by field-evaporation. These observations are clearly illustrated in fig. 4, which shows a sequence of mass spectra recorded while pulse field evaporating through the damaged region of tip #4. Each histogram represents the sum of $\approx$15 single-pulse field-desorption mass spectra, and each successive plot corresponds to a region $\approx$15 Å deeper into the bulk (i.e. about three pulses were used to remove each successive (110) plane). All species residing

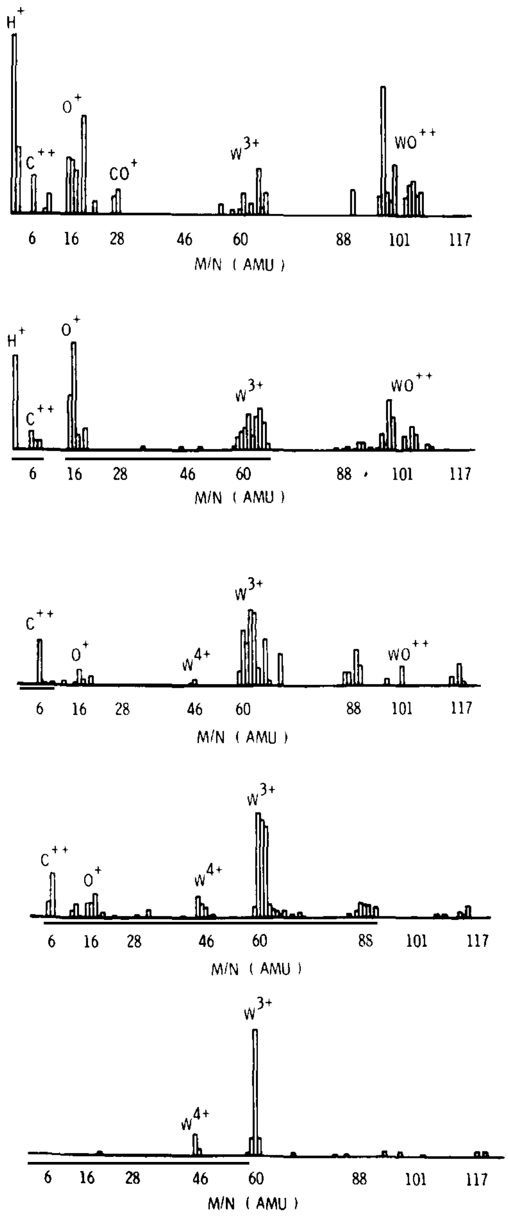

Fig. 4. A sequence of mass spectra obtained from the imaging atom-probe which shows the relative abundance of species residing within the damaged region of tip #4 as a function of depth into the bulk. The first spectra was recorded after the field-ion image of fig. 3b was obtained and each successive plot represents the abundance of the various species found ≈15 Å deeper into the lattice.

on the surface of the emitter had been removed prior to this sequence. It is clear from this figure that there are species other than the bulk tungsten which reside within the damaged region and that these species decrease in abundance the deeper into the lattice one probes. It can therefore be concluded that tungsten exposed to the operating conditions present in PLT at the time of exposure suffered noticeable lattice damage to within a very shallow depth from the surface. All plasma interactions with the tungsten occurred within this region, while the tungsten lattice beneath the damaged region was undisturbed.

In addition to the field-ion/field-desorption studies, Auger electron spectroscopy was used to analyze the surface of the stainless-steel sample holder cap *. The motivation for this analysis came from an observation of a visible deposit on one side of the holder after its return from PLT exposure. Figs. 5a and 5b show two sputter Auger depth profiles, one for the side of the cap on which the film was present (fig. 5a) and the other for the clean side (fig. 5b). A comparison of the two profiles suggests that the observed film was composed of primarily carbon, oxygen, iron and tungsten. Since the only source of tungsten in PLT was the limiters, it does appear that substantial amounts of limiter material entered the plasma and was subsequently deposited on the wall. Auger analysis cannot distinguish between various oxides, so that possible oxides of tungsten could not be observed. However, their presence is indicated by the field-desorption spectra of fig. 4 in which mass peaks identified with tungsten oxide decrease in abundance as the layer deposited on the tip #4 was probed in depth.

The results of the analysis of the first set of samples demonstrated that high-field techniques can be used to gain both qualitative and quantitative information on the plasma–wall interaction, and further indicated that field-ion microscopy and imaging atom-probe mass spectroscopy do, in fact, offer a unique perspective on the microscopic changes which occur at tokamak-irradiated sample surfaces. However, because this was a study primarily intended to establish the feasibility of using field-ion/desorption techniques, a number of questions remained. For example, what was the exact shape of each emitter tip before PLT exposure, and what changes occurred as a result of exposure? Also, were the oxides of tungsten observed due to a reaction between implanted oxygen and the lattice, or due to the implantation of tungsten oxide into the tungsten lattice? And, finally, what was the mechanism responsible for the damage observed to take place on the exposed samples? In an attempt to answer these questions, a second more carefully controlled experiment was undertaken.

3.2. Sample set #2

The second set of samples consisted of four tungsten and four rhodium tips arranged in a sample holder similar in design to the one used for the first set, but con-

---

* The AES measurements were carried out by D. Kramer and G. Nelson, Sandia Laboratories, Albuquerque, NM, USA.

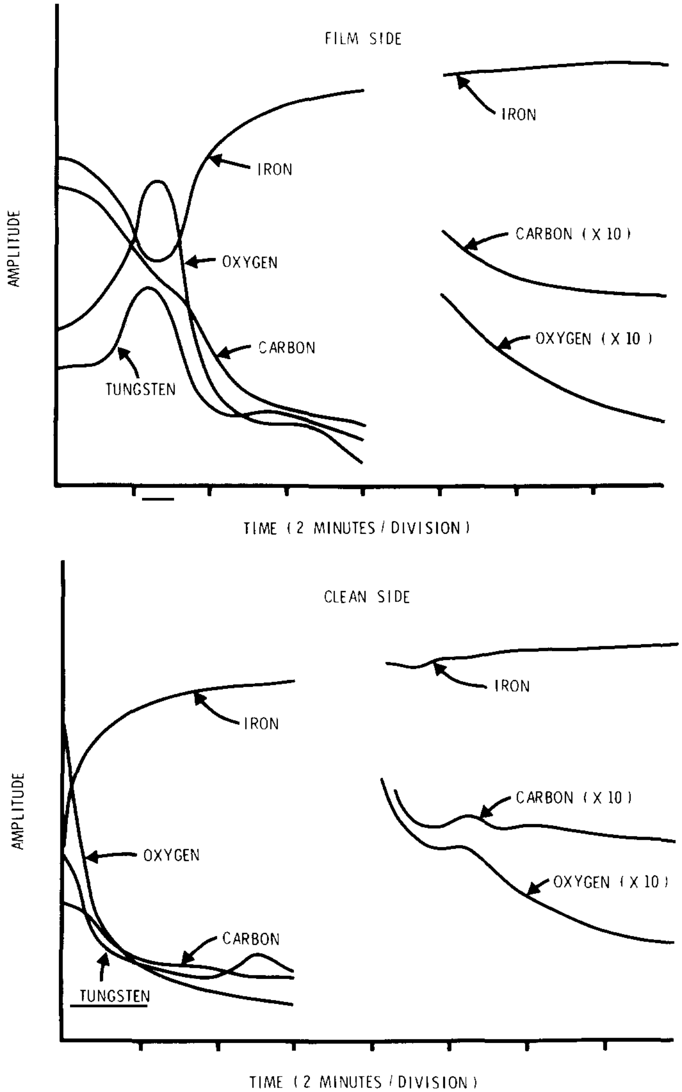

Fig. 5. Sputter-Auger depth profiles for the stainless-steel sample holder cap. The sputtering rate was approximately 50 Å/min. (a) Profile for the side of the cap where a visible metallic film was observed. (b) Profile for the opposite side which was free of visible deposits.

structed so that the tips were placed behind apertures of different diameters. Instead of using four identical apertures 1.5 mm in diameter as in the first set, two of the exposed tips were placed behind 1.5 mm diameter apertures and four were placed behind 0.5 mm diameter apertures. The remaining two tips were shielded from direct plasma exposure. This arrangement was used in an attempt to distinguish between two possible mechanisms which could have been responsible for the lattice damage observed on the exposed tips of the first set. The first (and, perhaps most obvious) explanation for the damage is that the surface atoms were removed or rearranged by the bombarding plasma species and impurities during the discharge or cleaning cycles (i.e., physical sputtering). A second possibility is that the plasma at the first wall may have entered the sample holder through the holes above the exposed tips causing electrical arcing between the plasma edge and the sharply pointed, grounded field emitters. The aperture diameters in the cap of the second set of tips would allow one to distinguish between these two mechanisms because the Debye length of the plasma (estimated to be of the order of 1.0 mm) would be larger than the diameter of the small apertures, and, therefore, the plasma would not be expected to enter the holder above those tips which were behind the 0.5 mm diameter apertures. Thus, damage observed only on the two samples placed behind large apertures (through which the plasma could enter) would suggest that electrical arcing was the responsible mechanism, whereas damage to all six exposed specimens would point to physical sputtering, since the aperture size would be expected to have no effect on the rate of sputtering for particles entering normal to the surface of the sample holder cover.

In order to quantitatively determine the extent of damage to the specimens by observing changes in specimen shape, and to determine the apex cone angle, transmission electron micrographs* at 250000 X magnification were taken of all eight samples before and after exposure in PLT. Within the resolution limits of the microscope ($\approx$10 Å), changes in the tip morphology resulting from irradiation could be determined unambiguously by this procedure.

The reason for including four rhodium samples in the second set was to try to determine if any significant amount of tungsten or tungsten-oxide was either deposited on the tip surface or implanted into its near-surface region during plasma exposure. The deposited layer found on the stainless steel sample holder of the first set indicated that significant amounts of tungsten and oxygen were escaping from the plasma; however, since all the sample tips were tungsten, it was impossible to distinguish between implanted or deposited tungsten and tungsten from the lattice itself. Any tungsten found on the surface or in the bulk of the rhodium samples would be easily detected and could help to determine the extent of tungsten contamination of the plasma by the tungsten limiters.

In order to eliminate the effects of discharge cleaning cycles, and minimize the cumulative damage due to repeated high power discharges, the exposure conditions for the second set of samples were made significantly different from those of the first set. First, the samples were exposed to only 69 high power deuterium discharges, with the holder and samples withdrawn and valved-off during discharge

---

* The TEM micrographs were taken by C. Hills, Sandia Laboratories, Albuquerque, NM on a JEOL Model JEM 100 electron microscope.

cleaning cycles. Hydrogen neutral beam injection was used in 39 of the 69 discharges. In addition, an experimental carbon limiter was used during this exposure interval, placed approximately 45° around the torus from the samples. As will be shown, the use of a carbon limiter was unfortunate, because it produced its own set of effects on the first wall and thereby made comparisons with the first sample set very difficult.

The samples of set #2 were labelled A through H. Table 1 lists the material and aperture size associated with each specimen. Fig. 6 shows electron micrographs of tips E, G, and H (representative of each aperture diameter used), taken before and after exposure. It is clear from this figure that material has been deposited on the surface of the samples after exposure to the plasma. It is also interesting to note the aperture size dependence of the thickness of the deposited layer. A consistent dependence on aperture diameter for all eight samples is evident in fig. 7. The layer on the two tips behind the large (1.5 mm diameter) apertures was measured to be ≈500 Å thick, on the samples behind the 0.5 mm apertures ≈50 Å, with no deposition observed on either shielded sample. A particle having a diameter ≈1200 Å can also be seen to be residing on tip E. There is no obvious correlation between substrate material and film thickness since samples A, B, C and H were made of tungsten and samples D, E, F and G were made of rhodium.

It should be noted that there was no change in the shape of the emitter substrate beneath the deposited layers visible in the electron micrographs. Field-ion images (discussed in a later section) confirmed this observation. The implications of these consistent observations will be discussed shortly.

The particle and deposited layer observed on tip E were first analyzed by a Kevex X-ray energy dispersive spectrometer while the sample was in the electron microscope. Unfortunately, because of the beryllium window on the spectrometer, it was not possible to detect species whose atomic number was less than 11. The STEM was put into its optional scanning mode, and when the beam was focused on the deposited layer alone, the X-ray spectrum showed only small amounts of Rh (the sub-

Table 1
Aperture diameters and field-ion imaging voltages for sample set #2

Specimen	Material	Aperture diameter (mm)	Ion imaging voltage (before exposure) (kV)	Ion-imaging voltage (after exposure) (kV)
A	W	1.5	5.7	6.0
B	W	0.5	5.8	5.8
C	W	0.5	6.0	5.8
D	Rh	0	7.7	8.0
E	Rh	1.5	4.0	6.0
F	Rh	0.5	7.0	7.0
G	Rh	0.5	11.2	10.9
H	W	0	6.0	5.8

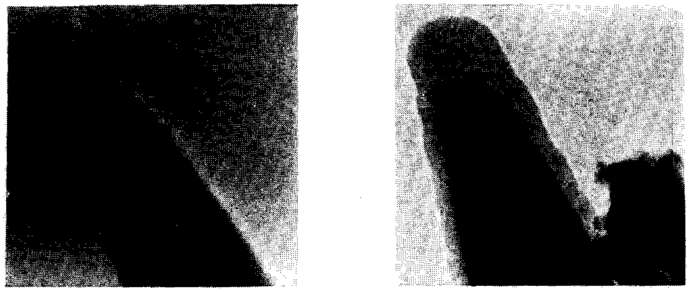

TIP E (BEFORE EXPOSURE) TIP E (AFTER EXPOSURE)

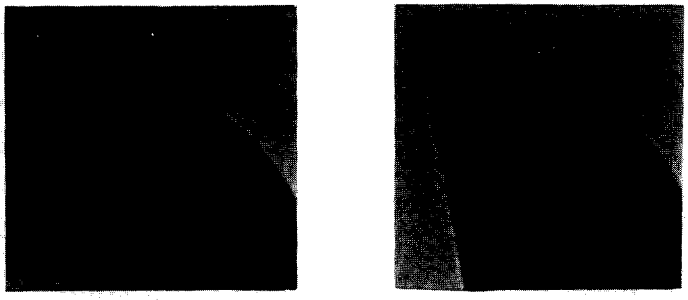

TIP G (BEFORE EXPOSURE) TIP G (AFTER EXPOSURE)

TIP H (BEFORE EXPOSURE) TIP H (AFTER EXPOSURE)

Fig. 6. Transmission electron micrographs of tips E, G, and H taken before and after exposure. Tip E was behind a 1.5 mm diameter aperture, tip G was behind a 0.5 mm aperture, and tip H was shielded during exposure. A surface layer of material is seen to have been deposited on the samples E and G as a result of plasma exposure.

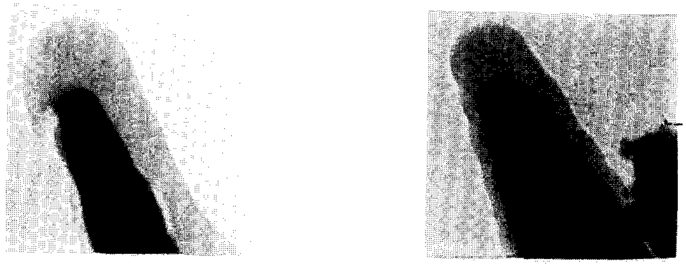

TIP A (LARGE APERTURE)

TIP E (LARGE APERTURE)

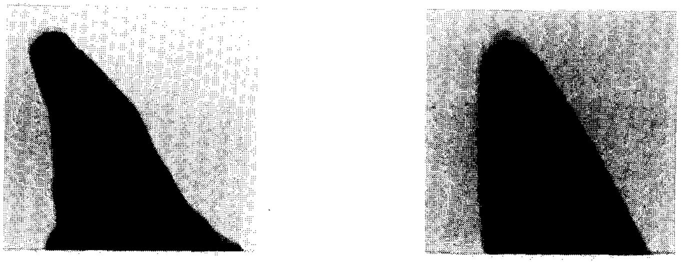

TIP B (SMALL APERTURE)

TIP F (SMALL APERTURE)

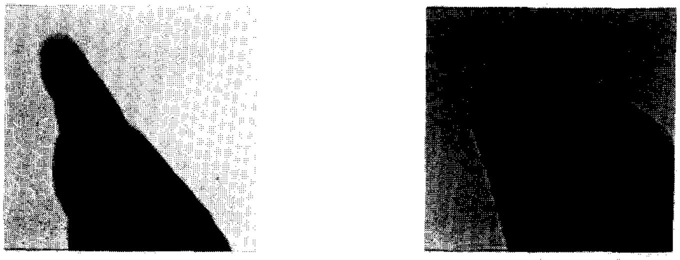

TIP C (SMALL APERTURE)

TIP G (SMALL APERTURE)

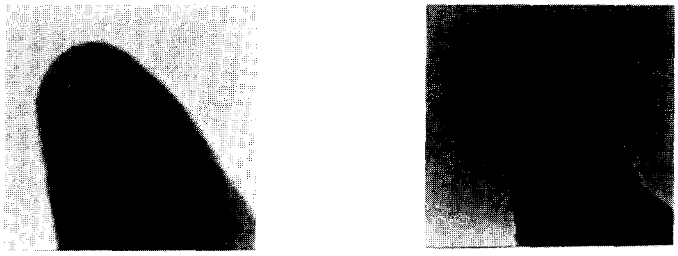

TIP D (SHIELDED)

TIP H (SHIELDED)

Fig. 7. Transmission electron micrographs of all samples of set #2 taken after exposure in PLT. Note the aperture-size dependence of the thickness of the deposited surface layer on the specimens.

strate material) and Cu, Cr, Fe and Ni (species characteristic of the stainless steel tip holder and other sample supporting structures in the STEM). The small signals detected from the layer suggested that the deposit had to be composed primarily of elements with atomic number <11. In view of the carbon limiter used, it is probable that the dominant layer species was carbon. When the beam was focused on the large particle (seen on the shank of tip E, fig. 7) very strong molybdenum peaks were observed in the X-ray spectrum. Presently, there is no satisfactory explanation for the presence of a deposited molybdenum particle on the tip shank.

Following the electron microscope measurements, the samples were further analyzed by field-ion microscopy and imaging atom-probe mass spectroscopy. The analysis procedure was the same for all of the specimens with the exception of tip E (see the following paragraph), and proceeded as follows. First, in order to analyze the composition of the surface layers deposited on the samples, mass spectra were recorded using a 1.0 kV desorption pulse, and no dc bias voltage. The dc voltage was then increased in steps of either 50 or 100 V, and spectra recorded until the specimen potential ($V_{dc} + V_p$) equaled the previously determined field-evaporation voltage of the specimen lattice. Next, a field-ion image was obtained and examined for structural damage on the tip surface. Finally, a depth profile into the near surface region was carried out with the spectrometer adjusted to detect only species with $m/n < 10$ (i.e., H^+, D^+, HD^+, He^+, C^{2+}).

In the analysis of tip E, the first step of the above procedure was eliminated, and a field-ion image was directly obtained without prior field-desorption to determine the nature of the deposited layer on the tip surface. Fig. 8 shows three field-ion images of tip E; the first taken before exposure in PLT, the second after exposure (following observation in the electron microscope, fig. 7), and the third after field-evaporation removal of the deposited surface layer. The second image in fig. 8 indicates that the deposited layer on the exposed tip was amorphous, or at least that it lacked regular crystal symmetry. It is interesting to note that a higher voltage was required for field-ion imaging of the specimen surface after exposure in PLT. This is a further indication of the presence of a deposited, non-metallic layer on the tip surface, since such a deposit would tend to lower the effective field strength and, therefore, require a higher voltage for imaging. Upon increasing the specimen potential, the deposited layer was observed (in the ion image) to be suddenly removed, therby producing a field at the surface of the tip which was much larger than the lattice evaporation field and causing either (1) rapid field-evaporation of the tip until the radius was increased sufficiently to compensate for the higher voltage or (2) the tip to "jump" to a larger radius configuration. For the case of tip E, it seemed that the latter occurred, because the voltage had to be increased even further to attain the final field-ion image shown in fig. 8 ($V = 6$ kV).

Field-ion micrographs of samples in set #2 taken both before and after irradiation in PLT are shown in figs. 9a and 9b. Even with the ångström resolution of the FIM, no structural damage was observed for any of the specimens of this set. Table 1 lists the voltages used for obtaining the field-ion images of the emitters. With the

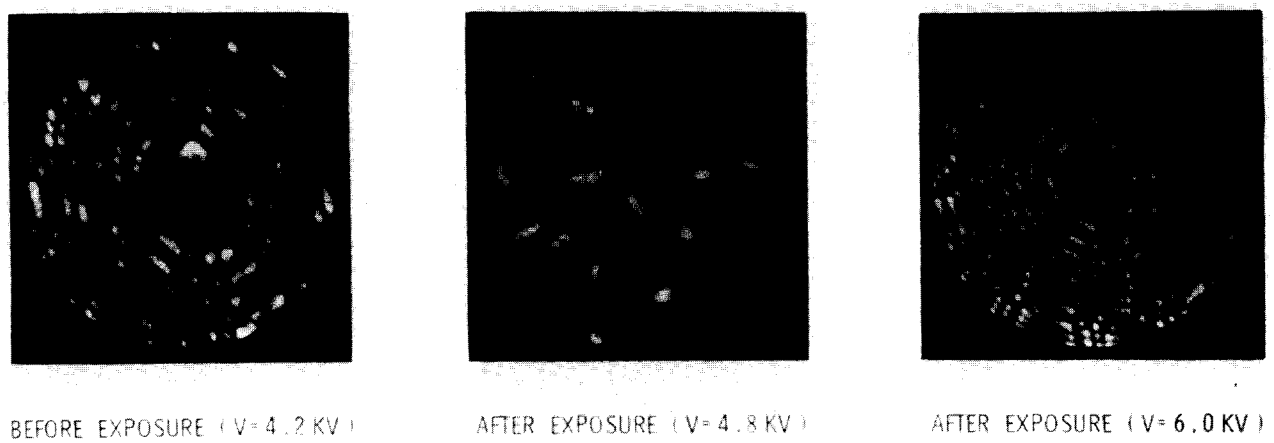

BEFORE EXPOSURE (V=4.2 KV)

AFTER EXPOSURE (V=4.8 KV)

AFTER EXPOSURE (V=6.0 KV)

Fig. 8. Field ion images (He, 26 K) of tip E of set #2 taken before exposure, after exposure with the deposited surface layer present, and after exposure with the surface layer removed.

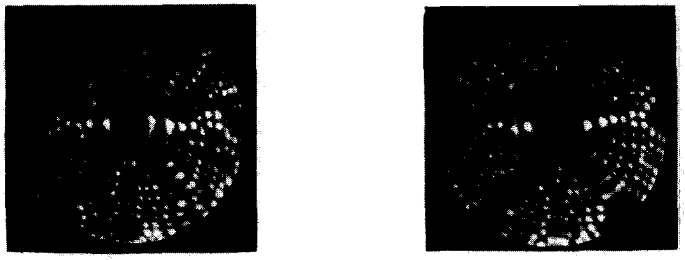

TIP A (BEFORE EXPOSURE) TIP A (AFTER EXPOSURE)

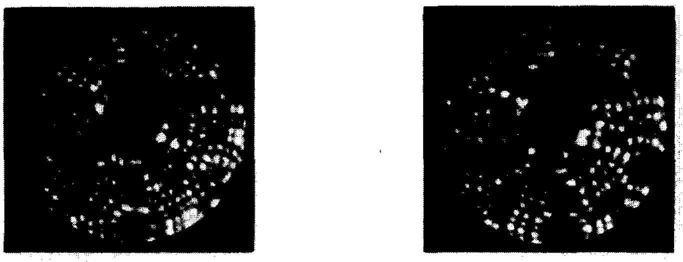

TIP B (BEFORE EXPOSURE) TIP B (AFTER EXPOSURE)

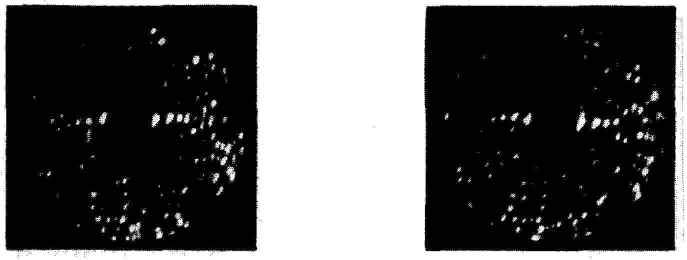

TIP C (BEFORE EXPOSURE) TIP C (AFTER EXPOSURE)

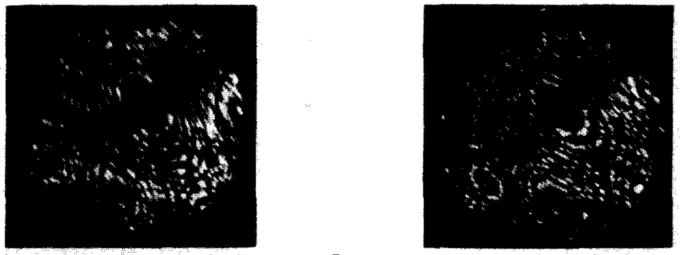

a

TIP D (BEFORE EXPOSURE) TIP D (AFTER EXPOSURE)

Fig. 9.(a) Field-ion micrographs (He, 26 K) of tips A–D of set #2 taken both before and after exposure in PLT.

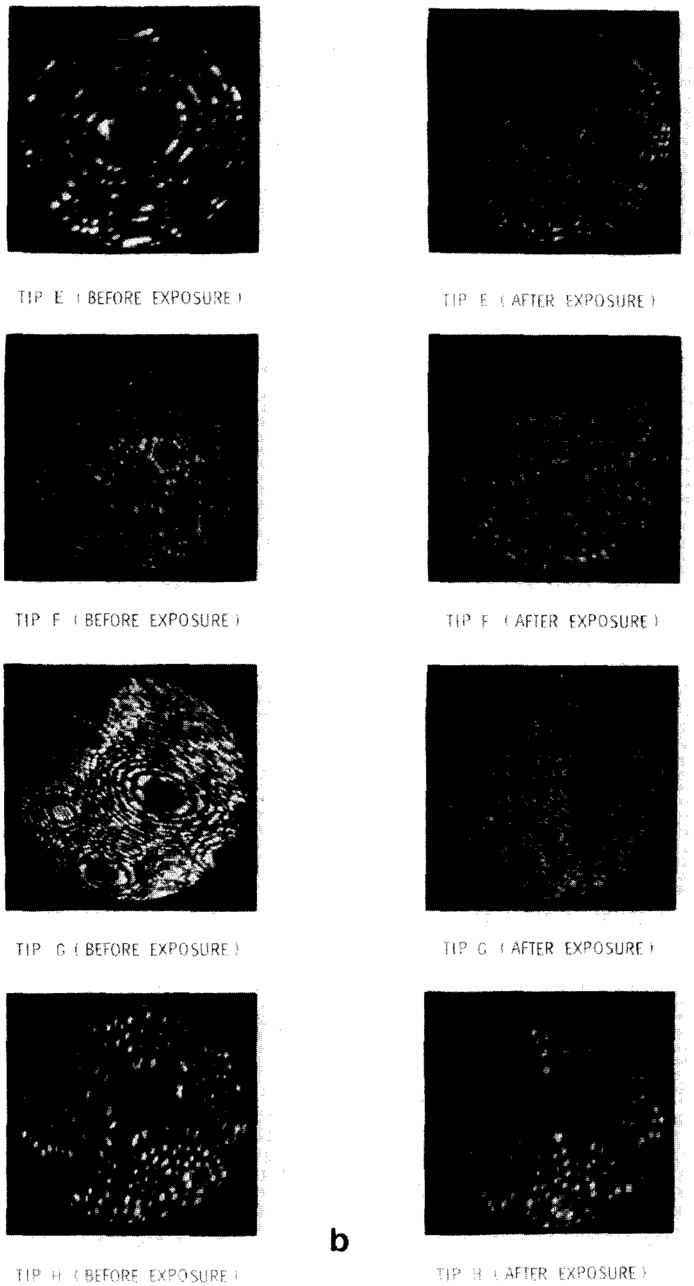

TIP E (BEFORE EXPOSURE)
TIP E (AFTER EXPOSURE)
TIP F (BEFORE EXPOSURE)
TIP F (AFTER EXPOSURE)
TIP G (BEFORE EXPOSURE)
TIP G (AFTER EXPOSURE)
TIP H (BEFORE EXPOSURE)
TIP H (AFTER EXPOSURE)

Fig. 9.(b) Field-ion micrographs (He, 26 K) of tips E–H of set #2 taken before and after exposure in PLT. No structural damage to the surface was observed for any of the samples of this set.

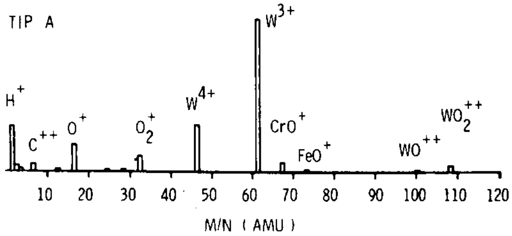

Fig. 10. Imaging atom-probe mass spectrum for species residing on the surface of tip A. The histogram represents the sum of over 100 single-pulse field-desorption spectra.

exception of tip E (see preceding paragraph) the ion imaging voltages were nearly identical before and after exposure, indicating that there was no change in radius of the tip as a result of the experiment [*].

A mass spectrum obtained from the imaging atom-probe mass analysis of the deposited surface layer on tip A is presented in fig. 10. The histogram shows the relative abundances of the different species detected while desorbing through the surface layer and a portion of the near-surface region. The plot shown represents the integration of over 100 single-pulse desorption spectra. One can deduce from these measurements that the layer on the surface contains tungsten, oxygen, carbon, deuterium and hydrogen. The amount of tungsten in the film was not as predominant as the histogram suggests, because a part of the near-surface region was sampled. However, tungsten did appear in the mass spectra even ar very low voltages, indicating that some quantity is present within the film. Since trapped hydrogen cannot be unambiguously separated from background hydrogen in the spectrometer its relative abundance may also be exaggerated. Trace amounts of wall material (i.e. Fe, Cr) in oxide form are also observed in the mass spectrum.

The question immediately arises as to why there is not more carbon relative to the other species in the mass spectra if the film is, in fact, composed mainly of carbon as the earlier X-ray analysis suggested. It is believed that the low abundance of carbon is an experimental artifact due to the removal of large portions of the film during a single desorption pulse. When a large number of ions are generated in a single desorption event, the amplifier measuring the signal from the detector becomes saturated so that true species amplitudes cannot be measured. This explanation is further substantiated by visual observation of desorption images having large image spot densities and occurring intermittently during the pulsed field-evaporation sequence. Thus, it appears to be difficult to use the imaging atom-probe technique as a true indicator of the relative abundance of species present within thick amorphous

---

[*] Tip A had a slightly higher imaging voltage in the micrograph taken after PLT exposure because pulse field-desorption was continued to a voltage higher than the original field evaporation voltage to ensure that the deposited surface layer was completely removed for analysis. Other discrepancies in the ion imaging voltages before and after exposure can be attributed to the subjective nature of determining a "best" field-ion image.

films on emitter surfaces unless some form of fast logarithmic amplifier can be developed to preserve the true amplitude of each desorbed species. However, the present data can still be used for a qualitative determination of the film composition. In the present study, the absence of species other than carbon, hydrogen, deuterium and oxygen in any significant amount in the mass spectra (combined with earlier X-ray fluorescence measurements showing a Z effective <11 for the film) is strong evidence that the observed film is composed primarily of carbon. The presence of a carbon limiter during exposure of these samples further defines a highly probable source for the observed carbon layer.

The mass spectra which were obtained from the analysis of the surface films on the other specimens were similar to the one in fig. 10 except that no W was seen on the Rh samples. This observation suggests that the W seen on the W samples was not coming from the plasma, but was being displaced from the bulk. This may not have been the case for the earlier sample set which was exposed with tungsten limiters in use.

Fig. 11 displays species abundance for tip A obtained from the imaging atom-probe and plotted as a function of the applied desorption voltage ($V_p + V_{dc}$). These plots show in a qualitative way the depth distribution of the various species through the deposited film. The large abundance at various points in the hydrogen spectra correlate with the voltages where large fractions of the film were removed (hydrogen abundance during such events did not, in general, saturate the amplifier). The presence of appreciable quantities of hydrogen within the film is interesting in view of the fact that hydrogen neutral beam injection was used in over half of the discharges to which the samples were exposed. Comparisons with proposed future experiments in which deuterium neutral beam injection will be employed should be useful in clarifying the role of neutral beam injection in the plasma–first wall interaction.

Depth profiles into the near-surface region of the specimen lattice in sample set #2 (beneath the deposited layer) did not show any implanted plasma species. Although this observation may, at first glance, seem somewhat surprising in view of earlier laboratory depth profiles for implanted deuterium [9], it can be explained in terms of the amorphous nature of the layer deposited on the sample surface during PLT exposure. The laboratory experiments were performed on clean, single crystal tungsten in which channeling of the implanted species was possible. Without channeling depth profiles are expected to be limited to several tens of ångströms, a depth much smaller than the thickness of the layers deposited on the PLT specimens. Another possibility is that implanted species may have diffused back to the surfaces during the time interval between PLT exposure and mass analysis (which was of the order of several months). Extrapolation of the high temperature diffusion coefficient for hydrogen in tungsten to room temperature [13] suggests, however, that the rates should be very low and implanted hydrogen or deuterium should not diffuse back to the surface.

The results obtained with the imaging atom-probe have been further substantiated with Rutherford ion backscattering measurements made on silicon and stain-

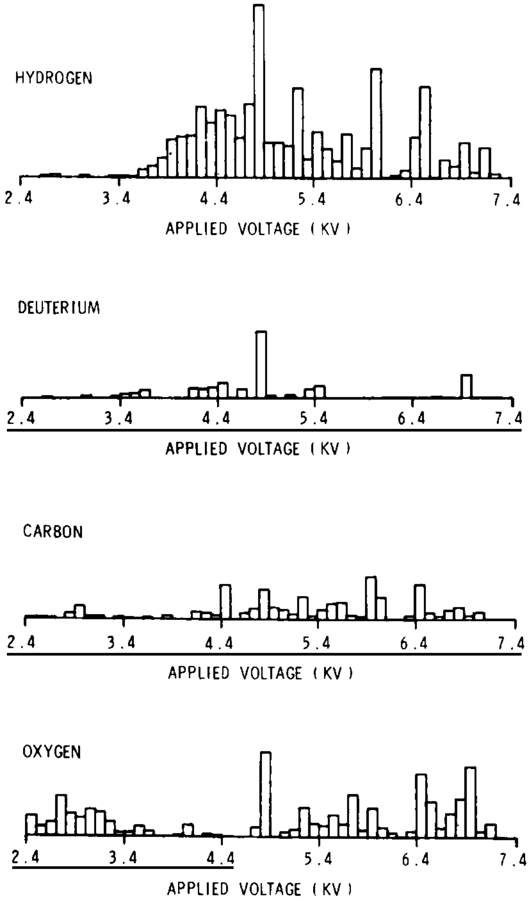

Fig. 11. Relative abundance of hydrogen, deuterium, carbon and oxygen plotted as a function of the applied desorption voltage ($V_p + V_{dc}$). The plots represent (qualitatively) the distribution of the species within the deposited surface layer.

less steel samples exposed at the same time as sample set #1 [14]. Although deuterium was observed to be implanted into the silicon samples exposed in PLT, the interpretation of the data suggested that it is trapped only because of a large number of damage centers in the lattice. Profiles measured for the stainless steel samples showed all the deuterium residing within 200 Å of the surface; a distance which would include the majority of any deposited layer, the thickness of which cannot be directly detected from the backscattering measurements.

4. Discussion

It has been shown that the techniques of field-ion microscopy and imaging atom-probe mass spectroscopy can be used as a plasma–first wall diagnostic in tokamak reactors. Even with the limited number of sample exposures performed, useful information has been obtained. For the first time, structural damage to the surface of specimens placed at the first wall has been observed with sufficient resolution to define the extent of damage on an atomic scale. Although the actual mechanism for the damage is still subject to question, it appears that even under extended operation of the tokamak, damage extends only of the order of tens of ångströms into sample substrates.

The absence of any observable damage on the surfaces of the exposed samples, as well as the different exposure conditions of set #2, does not permit any deduction to be made about the mechanism responsible for the damage seen in the first sample set. However, the fact that none of the samples in set #2 were damaged tends to rule out electrical arcing, since the occurrence of arcing should be independent of the exposure conditions (there were fewer discharges and no cleaning cycles during the exposure of the second sample set). It is, of course, possible that the damage observed in the first sample set was due physical sputtering during the low power discharge cleaning cycles seen by the samples. Clearly, more data from future samples exposed just to cleaning cycles, or just to high power discharges will be needed to elucidate the specimen damage mechanism.

When a carbon limiter was employed, the bulk of the first-wall–plasma interaction was found to occur within a contaminant layer deposited onto the samples during exposure to the plasma. If confirmed, this result implies that the nature of any deposited surface layer on the first-wall may be of greater importance in determining the extent of plasma–first-wall interaction than the material of which the wall is constructed. It should not be implied from the measurements reported here that a 200–500 Å layer of limiter material is uniformly deposited over the entire first-wall surface, since the deposition may actually be highly directional (as suggested by several of the electron micrographs of fig. 7). But it does appear that plasma instabilities causing partial vaporization of the limiter is the present, major contributor to impurities on the first wall of PLT. In fact, it is likely that for certain limiter materials under certain machine conditions (for example, those which produced the deposited layers observed here), limiter material deposited on the first wall will define a new first wall surface whose composition and properties can be drastically different from those of the original substrate.

An important observation to be noted is that no deposition could be detected on samples which were shielded from direct exposure to the plasma (control samples). As a result, it is known that in situ exposure to the reactor ambient is not, itself, the source of major first wall contamination, but that the wall must be exposed in a line-of-sight fashion to the plasma if contamination is to be appreciable. The observed aperture size dependence of the thickness of the deposited layer (shown in fig. 7) suggests that either a nonparallel influx of impurities with respect to the axis of the samples occurred, or, if the impurities were charged, a focusing effect due to the electrostatic fields produced by the potential difference between the plasma edge and grounded emitters was responsible. More data will be required to resolve this uncertainty.

The absence of implanted plasma species in the near-surface region of the undisturbed lattice (beneath the deposited layer) in either sample set, effectively eliminated the possibility of measuring depth profiles of low energy plasma species. As a result, it was impossible to determine the energy distributions of escaping plasma species by comparing in situ profiles with those obtained previously in the laboratory. Since the ability to record depth profiles in the substrate lattice appears to be limited only by the presence of deposited contamination layers (or damage to the lattice due to arcing or sputtering), energy distribution measurements will have to wait until first-wall–plasma interactions of this type can be minimized. Since the contaminant layers observed in the second sample set were probably due to the experimental carbon limiter used and, therefore, may not be characteristic of "normal" machine operation, future energy distributions measurements may indeed be possible. By "valving-off" the samples to eliminate cleaning-cycle and neutral beam injection effects, and by choosing appropriate sample apertures for plasma exposure, substrate damage due to sputtering (or arcing) can also, in principle, be eliminated, thereby increasing the probability of obtaining depth profiles of plasma species with ångström depth resolution.

References

[1] Tokamak Impurity Report, DOE/ET001, December 1977.
[2] S.A. Cohen, J. Vacuum Sci. Technol. 13 (1976) 449.
[3] S.A. Cohen, Proc. 3rd Internat. Conf. Plasma–Surface Interactions in Controlled Fusion Devices, Culham, England (April, 1978), J. Nucl. Mat., to be published.
[4] J.A. Panitz, Imaging Atom-Probe Mass Spectroscopy, Prog. Surface Sci. 6 (1978).
[5] E.W. Müller and T.T. Tsong, Field Ion Microscopy, Principles and Applications (Elsevier, Amsterdam, New York, 1969).
[6] Annual Proc. Electron Microscope Society of America (1970–1978).
[7] S.A. Cohen, PPPL Report #MATT-1171 (1975).
[8] J. Lindhard, Kgl. Danske Videnskab. Selskab Mat. Fys. Medd. 28 (1954).
[9] J.A. Panitz, J. Vacuum Sci. Technol. 14 (1977) 502.
[10] J.A. Panitz, CRC Crit. Rev. Solid State Sci. 5 (1975) 153.
[11] J.A. Panitz, J. Nucl. Mat. 63 (1977) 477.
[12] S. Kapur and E.W. Müller, Surface Sci. 66 (1977) 45.
[13] R.E. Stickley, in: Chemistry of Fusion Technology, ed. D.M. Gruen (Plenum Press, New York, 1972) p. 241.
[14] J.A. Borders, Proc. 3rd Internat. Conf. Plasma–Surface Interactions in Controlled Fusion Devices, Culham, England (April, 1978) J. Nucl. Mat., to be published.